The Effect of Templating on the Mechanical Properties of Smectic Liquid Crystal Elastomers

S. R. Berrow[1*], T. Raistrick[1], A. Street[1], E. J. Cooper[1], M. Coleman[1], R. J. Mandle[1,2], and H. F. Gleeson[1]

[1]School of Physics and Astronomy, University of Leeds, LS2 9JT

[2]School of Chemistry, University of Leeds, LS2 9JT

*S.R.Berrow@leeds.ac.uk

Electronic Supplementary Information

Supporting Information available: Experimental information, synthetic procedures for the synthesis of all intermediates and monomers synthesised, confirmation of sample alignment via optical microscopy, X-ray scattering data, differential scanning calorimetry thermograms for cured LCEs, Mechanical analysis and interpretation.

Table Of Contents

Experimental Information

Flash Chromatography

Flash chromatography was performed on a Combiflash NextGen 300+ system (Teledyne Isco) using silica gel as a stationary phase (Modus B, Chromatography Direct), an appropriate mobile phase as specified in the experimental procedure, and detection in the 200-800 nm wavelength range.

Structural Analysis

Nuclear magnetic resonance (NMR) spectra were recorded using a Bruker AVANCE III (400 MHz) NMR spectrometer (Bruker UK Ltd., Coventry, UK) at 298 K and referenced to TMS. NMR spectra were viewed and analysed using MNova NMR software.

Accurate Mass spectra were acquired on a Bruker Impact II QqTOF spectrometer equipped with a VIPHESI source using electrospray ionisation. Samples were introduced using an HTC PAL autosampler and Bruker Elute Pump. HPLC columns were heated to 40 °C unless otherwise stated. Samples passed through a Bruker Diode array UV-detector before entering the mass spectrometer. Calibration was performed by infusion of 5mM sodium formate solution at the end of each acquisition. Samples were submitted as solutions in acetonitrile at 10 µg/mL concentration, and data were collected in positive mode.

Thermal Analysis

Differential scanning calorimetry (DSC) measurements were performed using a TA Instruments Q2000 DSC instrument (TA Instruments, Wilmslow UK), equipped with a RCS90 Refrigerated cooling system (TA Instruments, Wilmslow UK). The instrument was calibrated against an Indium standard, and data were processed using TA Instruments Universal Analysis Software. Samples were analysed under a nitrogen atmosphere, in hermetically sealed aluminium TZero crucibles (TA Instruments, Wilmslow, UK) and subjected to three analysis cycles.

For the analysis of the uncured LCE mixtures, each cycle consisted of: a heating phase from 0–100 °C at a heating rate of 10 °C/min; an isothermal phase at 100 °C for 2 minutes; a cooling phase from 100–0 °C at 10 °C/min; and an isothermal phase at 0 °C for 2 minutes. Clearing temperatures are reported as onset values.

For LCE analysis, each cycle consisted of: a heating phase from -50–150 °C at a heating rate of 10 °C/min; and isothermal phase at 150 °C for 2 minutes; a cooling phase from 150 – -50 °C at 10 °C/min; and an isothermal phase at -50 °C for 2 minutes. The glass transition temperatures of the polymers were recorded as the onset value, on the heating phase of the second cycle.

Optical Microscopy

Polarised light optical microscopy (POM) was performed using a Leica DM2700P polarised light microscope (Leica Microsystems (UK) Ltd., Milton Keynes, UK), equipped with 10x and 50x magnification, and a rotatable stage. For LCE samples, the films were mounted on a glass slide, and analysed under ambient conditions, using 10x magnification. For phase identification of the liquid crystal precursor mixtures, a Mettler Toledo FP82HT Hot Stage (Mettler-Toledo Ltd., Leicester, UK), controlled by a Mettler Toledo FP90 central processor (Mettler-Toledo Ltd., Leicester, UK) was used to control the temperature of the sample with a relative accuracy of 0.1 °C. In this case, the sample was mounted between a glass microscope slide and a glass cover slip, and samples were analysed using 50x

magnification. Images were recorded using a Nikon D3500 Digital Camera (Nikon UK Ltd., Surbiton, UK), using DigiCamControl software.

Conoscopy was performed on homeotropic LCE films using a Leica DM 2700P polarizing microscope in transmission mode under cross-polarized conditions. The microscope was equipped with a 0.9 numerical aperture (NA) condensing lens and a 0.95 NA 80x Leitz microscope objective. To study the conoscopic patterns, a Bertrand lens was inserted between the microscope objective and the eyepiece. The conoscopic patterns were captured with a Nikon D3500 camera. The homeotropic sample is held under strain with Kapton tape and allowed to stress relax for two minutes before the image of the conoscopic pattern is recorded. The strain is applied parallel to the analyzer of the cross-polarized microscope and measured with digital callipers.

X-Ray Scattering Measurements

2D Small angle (SAXS) and wide angle (WAXS) X-ray scattering experiments were performed on an Anton Paar SAXSpoint 5.0 system (K-α Cu source, λ=1.5418 Å) with a Dectris EIGER2 R 1M (1028 pixel x 1062 pixel array). Measurements were performed at room temperature on 100 μm (nominal thickness) LCE samples averaging 3 frames with exposures times of 300 s. A 2 mm beam size was used and the measurements were run using a beamstop. A background scan was performed for both the SAXS and WAXS detector position which was subtracted from the measurements to minimise contributions from intrinsic background scattering and the Mylar protective film in front of the detector. 2D data reduction was performed by radially integrating the 2D patterns whilst masking the central contribution related to the non-scattered X-ray beam.

The correlation lengths parallel ($\xi_{\|}$) to the director were calculated, according to **Equation S1**, as was recently used by Kennedy *et al* for LCEs.[1] This equation uses the full width half maximum ($w_{\|}$) of Gaussian fittings to the scattering intensity of the q ~ 1.6 nm^{-1} feature (the (001) Bragg peak due to the smectic layer spacing).

$$\xi_{||} = \frac{2\pi}{w_{||}} \quad \textbf{(S1)}$$

Mechanical Analysis

The macroscopic shape changes upon the application of strain were observed using bespoke equipment designed and manufactured in-house, full specifications for which can be found in previous work. [2,3] This apparatus consists of two actuators and a load cell, enclosed within a temperature-controlled environment, and is equipped with optics that enable images of the sample to be recorded both via optical microscopy and polarising optical microscopy simultaneously. In this work, samples of 20 mm x 2 mm were analysed at room temperature. The initial gap between the actuators was 16.5 mm, and the samples were subject to strain steps of 0.5 mm at 10-minute intervals, until the sample failed. The samples were strained perpendicular to the initial director, as displayed in Figure 5 in the article text.

Stress-strain curves were recorded based on tensile measurements performed on a TA Instruments DMA 850 (TA Instruments, Wilmslow UK), and the data processed using TRIOS software. Samples of dimensions approximately 10 mm x 2 mm x 100 μm were subject to temperature sweeps using film clamps. Samples were subject to strain at a rate of 0.306 mm/minute at room temperature until sample failure.

Synthetic Procedures

General Procedure for the Synthesis of 4-((6-(acryloxy)hexyl)oxy)phenyl Benzoate Monomers

The synthetic procedure for the synthesis of 4-((6-(acryloxy)hexyl)oxy)phenyl 4'-cyanobenzoate is given as a representative example. To dichloromethane (200 mL) was added 6-(4-hydroxyphenoxy)hexyl acrylate (3.00 g, 11.3 mmol), 4-cyanobenzoic acid (1.50 g, 10.2 mmol), N-(3-Dimethylaminopropyl)-N′-ethylcarbodiimide hydrochloride (2.17 g, 11.3 mmol) and 4-Dimethylaminopyridine (0.14 g, 1.13 mmol). The resulting solution was stirred overnight at room temperature. The solvent was then removed under reduced pressure. The crude product was purified over silica gel using a hexane:ethyl acetate gradient as the eluent. Upon removal of the solvent, the resulting solid was recrystallized from ethanol, to yield the product as colourless crystals of mass 1.68 g (42% yield).

4-((6-(acryloxy)hexyl)oxy)phenyl 4'-cyanobenzoate

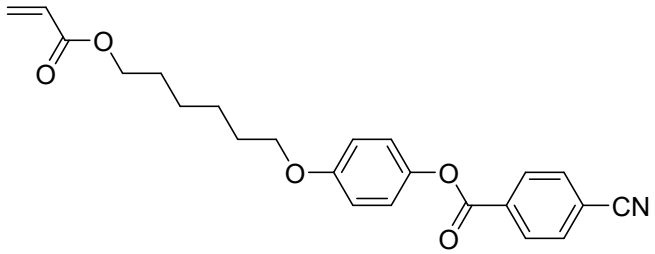

^{1}H NMR (400 MHz, $CDCl_3$) δ: 8.22 (ddd, 2H, *J*= 8.9, 3.0, 2.2 Hz, Ar-H), 7.73 (ddd, 2H, *J*= 8.9, 3.0, 2.2 Hz, Ar-H), 7.05 (ddd, 2H, *J*= 8.9, 3.0, 2.2 Hz, Ar-H), 6.86 (ddd, 2H, *J*= 8.9, 3.0, 2.2 Hz, Ar-H), 6.33 (dd, J = 17.3, 1.5 Hz, 1H, $=CH_2$), 6.05 (dd, J = 17.3, 10.4 Hz, 1H, -CH=), 5.75 (dd, J = 10.4, 1.5 Hz, 1H, $=CH_2$), 4.11 (t, J = 6.7 Hz, 2H, -O-CH_2-), 3.90 (t, J = 6.4 Hz, 2H, -O-CH_2-), 1.80 – 1.59 (m, 4H, -CH_2-), 1.51 – 1.32 (m, 4H, -CH_2-).

^{13}C{^{1}H} NMR (101 MHz, $CDCl_3$) δ: 166.33 (C=O), 163.94 (C=O), 157.15 (Ar C-OR), 143.88 (Ar C-OR), 133.55 (Ar -C), 132.38 (Ar -C), 130.61 (Ar -C), 130.55 (C=C), 128.60 (C=C), 122.16 (Ar -C), 117.89 (Ar -C), 116.92 (-C≡N), 115.20 (Ar -C), 68.23 (-O-CH_2-), 64.51 (-O-CH_2-), 29.14 (-CH_2-), 28.58 (-CH_2-), 25.76 (-CH_2-).

4-((6-(acryloxy)hexyl)oxy)phenyl 4'-isothiocyanatobenzoate

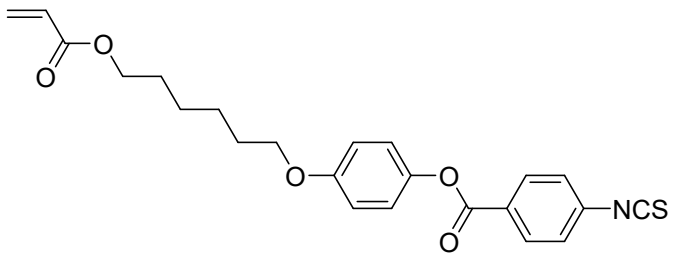

^{1}H NMR (400 MHz, $CDCl_3$) δ: 8.15 – 8.05 (m, 2H, Ar-H), 7.29 – 7.22 (m, 2H, Ar-H), 7.07 – 6.99 (m, 2H, Ar-H), 6.89 – 6.81 (m, 2H, Ar-H), 6.33 (dd, J = 17.3, 1.5 Hz, 1H, -C=CH_2), 6.05 (dd, J = 17.3, 10.4 Hz, 1H, -CH=C), 5.75 (dd, J = 10.4, 1.5 Hz, 1H, -C=CH_2), 4.11 (t, J = 6.6 Hz, 2H, -O-CH_2), 3.89 (t, J = 6.4 Hz, 2H, -O-CH_2), 1.69 (m, 4H, -CH_2-), 1.51 – 1.32 (m, 4H, -CH_2-).

$^{13}C\{^{1}H\}$ NMR (101 MHz, $CDCl_3$) δ: 166.34 (C=O), 164.39 (C=O), 156.97 (Ar C-OR), 144.09 (Ar C-OR), 138.23 (Ar C), 136.25 (Ar C), 131.62 (Ar C), 130.55 (C=C), 128.61 (C=C), 128.19 (-NCS), 125.83 (Ar C), 122.38 (Ar C), 122.29 (Ar C), 115.15 (Ar C), 68.21 (-O-CH_2-), 64.53 (-O-CH_2-), 29.16 (-CH_2-), 28.58 (-CH_2-), 25.77 (-CH_2-).

4-((6-(acryloxy)hexyl)oxy)phenyl 4'-(4''-propylcyclohexyl)*trans*-cyclohexanoate

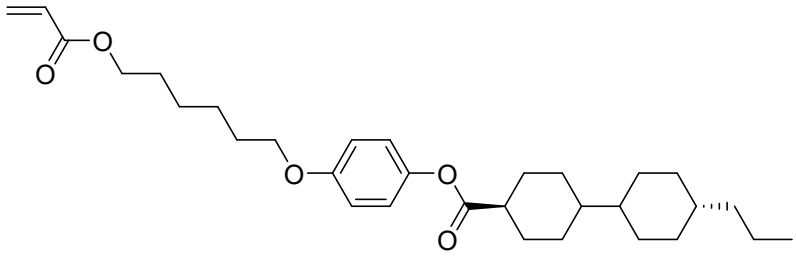

^{1}H NMR (400 MHz, $CDCl_3$) δ: 6.97 – 6.67 (m, 4H, Ar-H), 6.32 (dd, J = 17.3, 1.5 Hz, 1H, -C=CH_2), 6.05 (dd, J = 17.3, 10.4 Hz, 1H, -CH=C), 5.74 (dd, J = 10.4, 1.5 Hz, 1H, -C=CH_2), 4.10 (t, J = 6.6 Hz, 2H, -O-CH_2-), 3.86 (t, J = 6.4 Hz, 2H, -O-CH_2-), 2.35 (tt, J = 12.2, 3.3 Hz, 1H, alkyl CH), 2.12 – 2.02 (m, 2H, alkyl CH), 1.91 - 1.58 (m, 11H, alkyl CH), 1.54 – 1.31 (m, 5H, alkyl CH), 1.24 (m, 2H, alkyl CH), 1.14 – 0.85 (m, 9H, alkyl CH), 0.80 (m, 5H, alkyl CH).

$^{13}C\{^{1}H\}$ NMR (101 MHz, $CDCl_3$) δ: 175.11 (C=O), 166.33 (C=O), 156.61 (Ar C-OR), 144.27 (Ar C-OR), 130.52 (C=C), 128.61 (C=C), 122.25 (Ar C), 114.98 (Ar C), 68.16 (O-CH_2-), 64.53 (O-CH_2-), 43.67, 43.26, 42.53, 39.80, 37.60, 33.54, 30.02, 29.32, 29.16, 28.57, 25.76, 20.05, 14.43 (alkyl C).

4-((6-(acryloxy)hexyl)oxy)phenyl 4'-(4''-ethyl-*trans*-cyclohexyl)benzoate

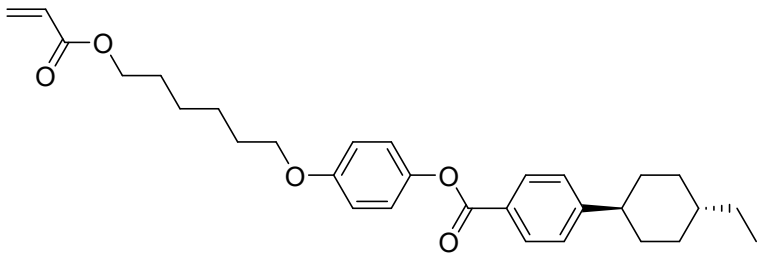

^{1}H NMR (400 MHz, $CDCl_3$) δ: 8.10 – 8.02 (ddd, J = 8.9, 2.8, 2.0 Hz, 2H, Ar-H), 7.21 – 7.13 (ddd, J = 8.5, 2.9, 1.8 Hz, 2H, Ar-H), 7.07 – 6.99 (ddd, J= 8.6, 2.6, 2.0 Hz, 2H, Ar-H), 6.92 – 6.84 (ddd, J= 9.0, 2.9, 2.1 Hz, 2H, Ar-H), 6.33 (dd, J = 17.3, 1.5 Hz, 1H, -C=CH_2), 6.05 (dd, J = 17.3, 10.4 Hz, 1H, -CH=C), 5.74 (dd, J = 10.4, 1.5 Hz, 1H, -C=CH_2), 4.11 (t, J = 6.6 Hz, 2H, -O-CH_2-), 3.97 (t, J = 6.4 Hz, 2H, -O-CH_2-), 2.41 (tt, J = 12.2, 3.3 Hz, 1H, alkyl CH), 1.80 (m, 6H, alkyl CH), 1.65 (m, 2H, alkyl CH), 1.54 – 1.30 (m, 6H, alkyl CH), 1.26 – 1.05 (m, 3H, alkyl CH), 1.05 – 0.90 (m, 2H, alkyl CH), 0.84 (t, J = 7.3 Hz, 3H, CH_3).

$^{13}C\{^{1}H\}$ NMR (101 MHz, $CDCl_3$) δ: 166.33 (C=O), 165.12 (C=O), 163.36 (Ar C-OR), 149.00 (Ar C-R), 145.28 (Ar C-OR), 132.26 (Ar C), 130.57 (C=C), 128.59 (C=C), 127.74 (Ar C), 121.86 (Ar C), 121.40 (Ar C), 114.25 (Ar C), 68.07 (O-CH_2), 64.48 (O-CH_2), 44.12, 39.09, 34.42, 33.18, 30.00, 29.01, 28.57, 25.75, 25.72, 11.55 (alkyl C).

LCE Sample Alignment

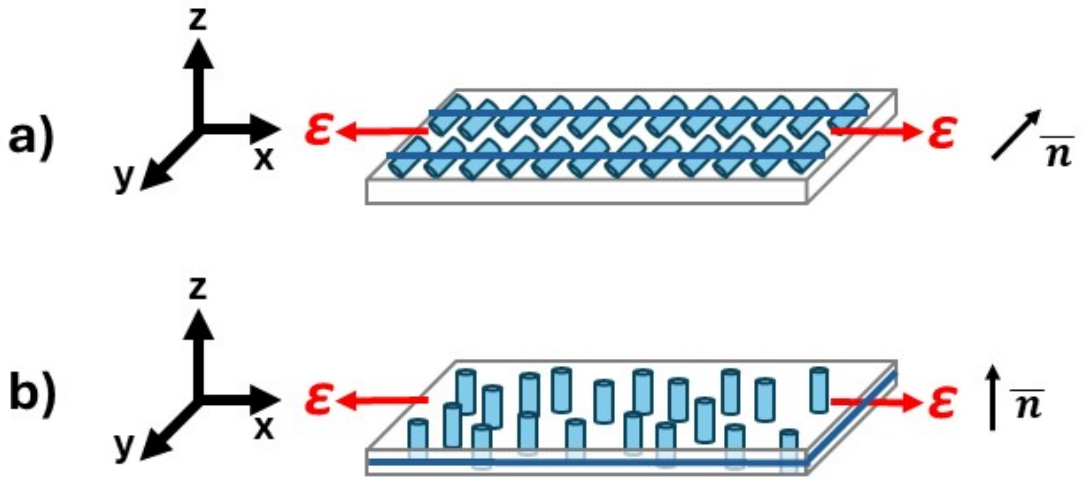

Figure S1 *– A schematic representation of the two alignment geometries employed in this work, with pale blue cylinders representing the mesogens, and dark blue lines representing the smectic layers. In both cases, ε represents the applied strain, and* $\bar{n}$ *represents the orientation of the director. Panel a) displays the samples fabricated with planar alignment (director oriented along the y-axis), and panel b) represents the samples made with homeotropic alignment (director oriented along the z-axis).*

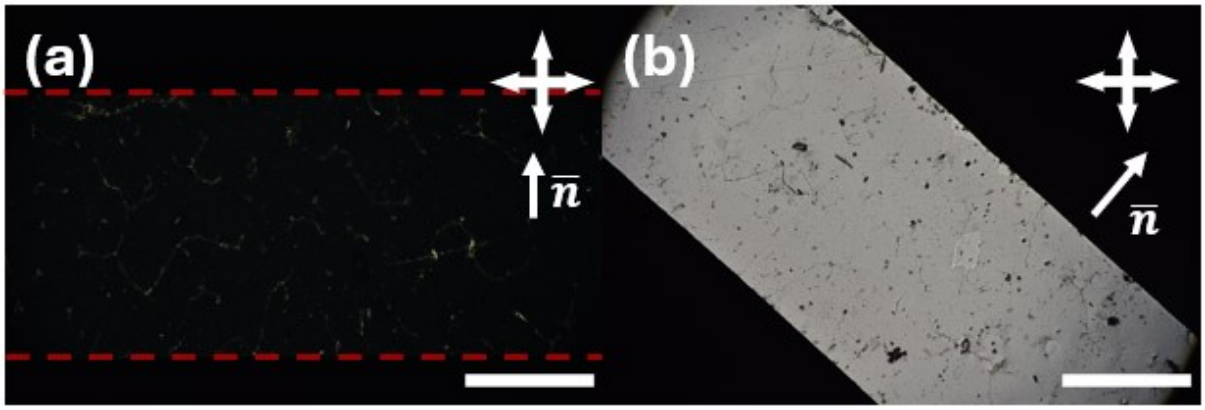

Figure S2 *- An example polarised optical microscopy image confirming planar alignment of the LCEs (in this case made with* ***M3****), showing a dark state when visualised under crossed-polarisers (a), which becomes a bright state when rotated about 45° (b). The scale bars represent 1 mm.*

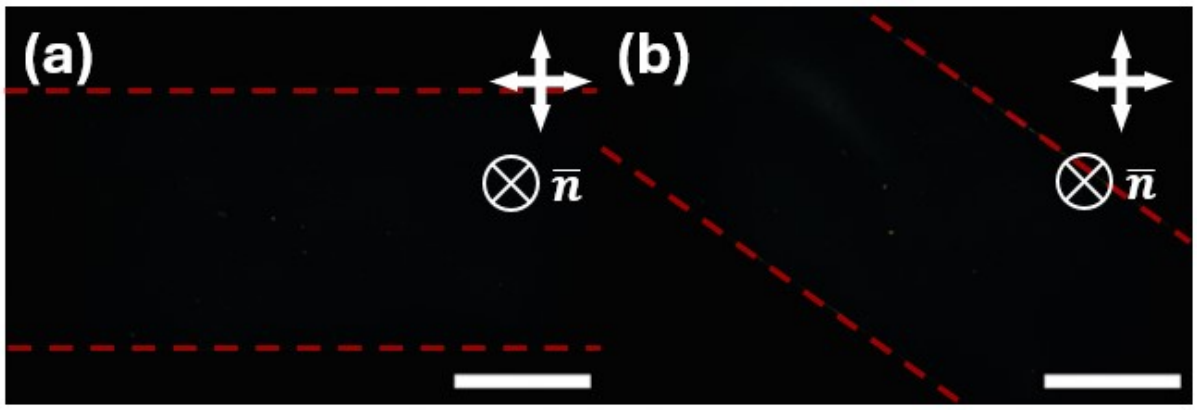

Figure S3 *– An example polarised optical microscopy image confirming homeotropic alignment of the LCEs (in this case made with* ***M3****), showing a dark state when visualised under crossed-polarisers (a), and retaining the dark state when rotated about 45° (b). The scale bars represent 1 mm.*

X-Ray Scattering

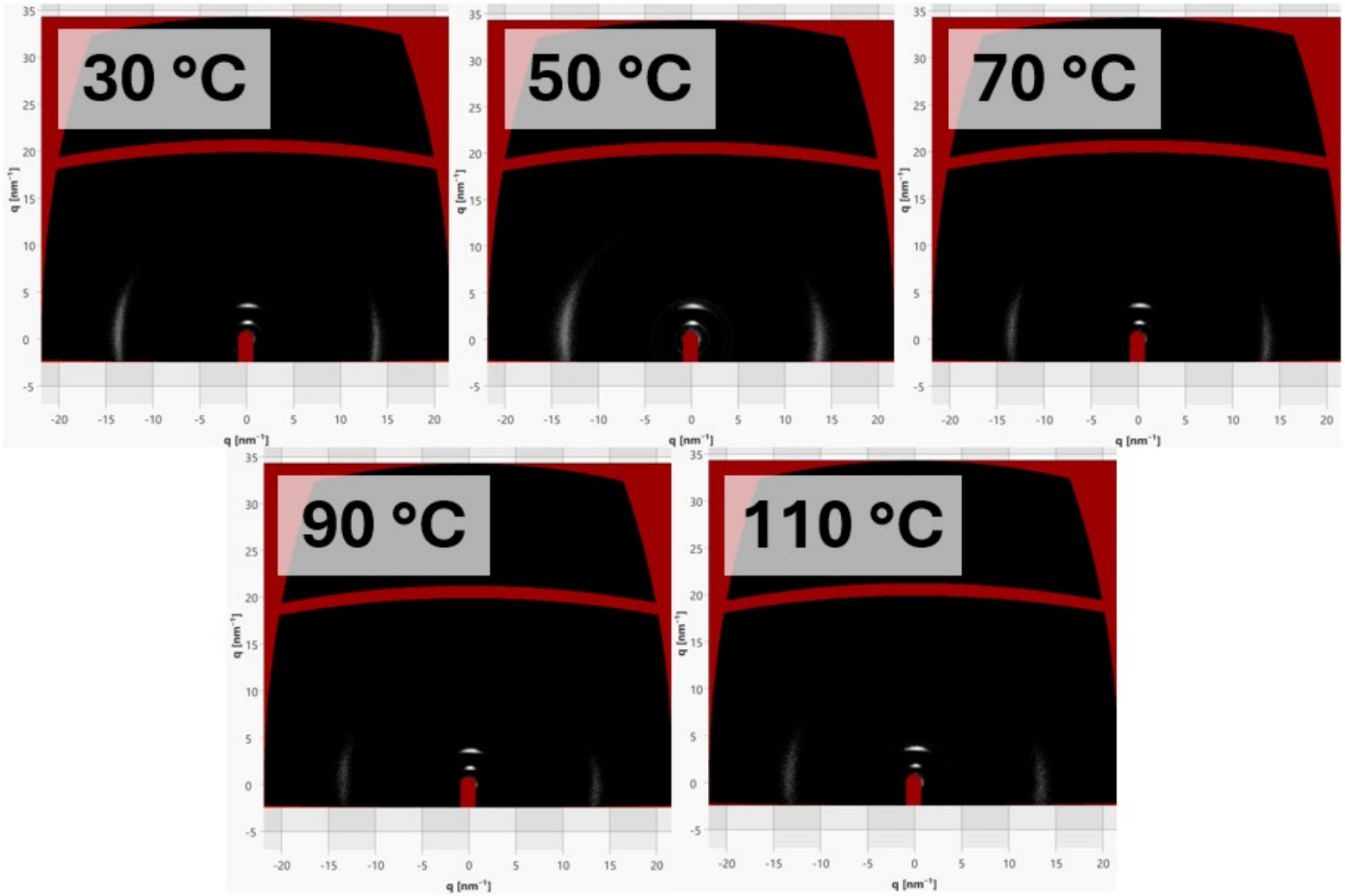

Figure S4 *– Representative 2D X-ray scattering patterns as a function of temperature for the M6 LCE.*

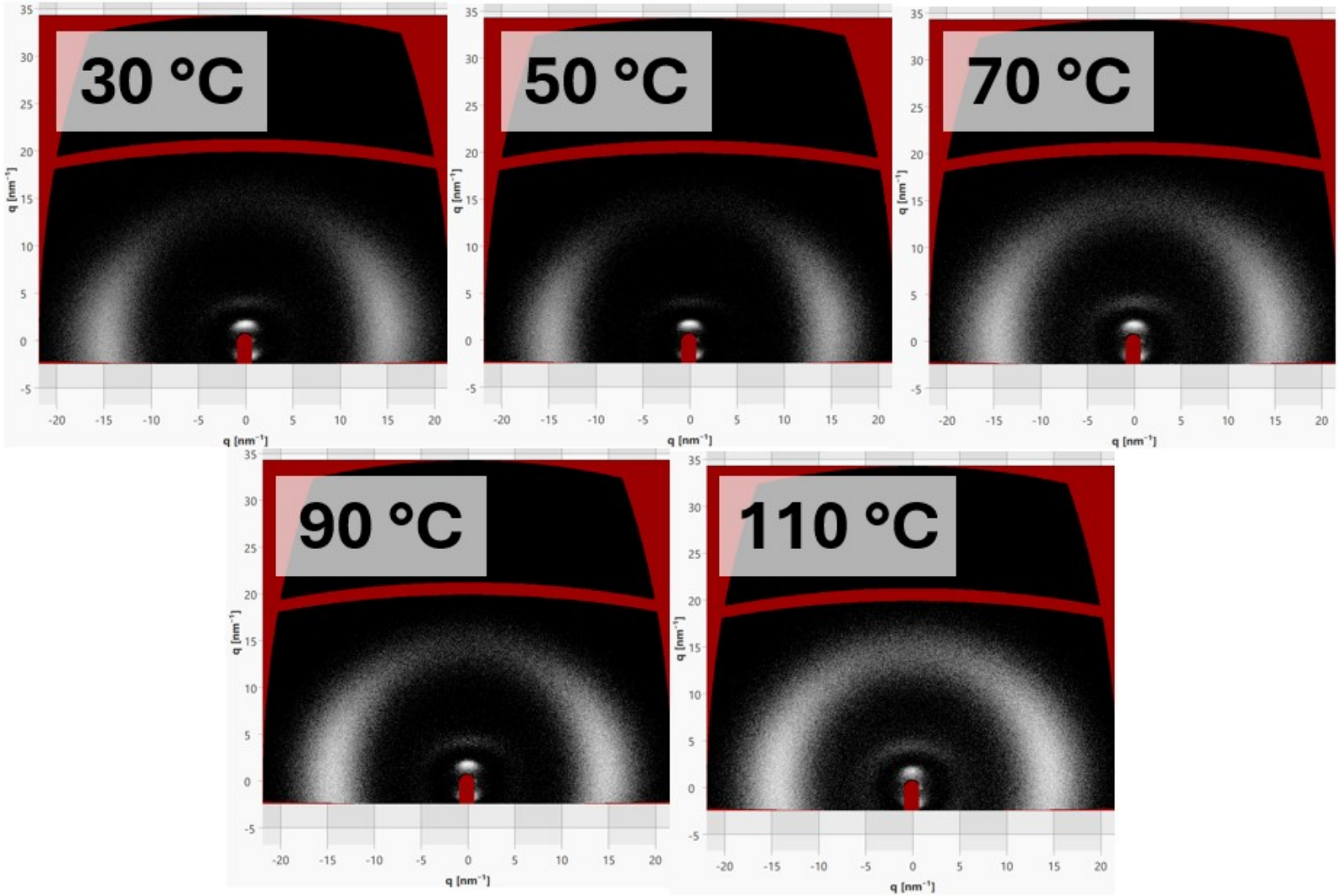

Figure S5 *– Representative 2D X-ray scattering patterns as a function of temperature for the M4 LCE*

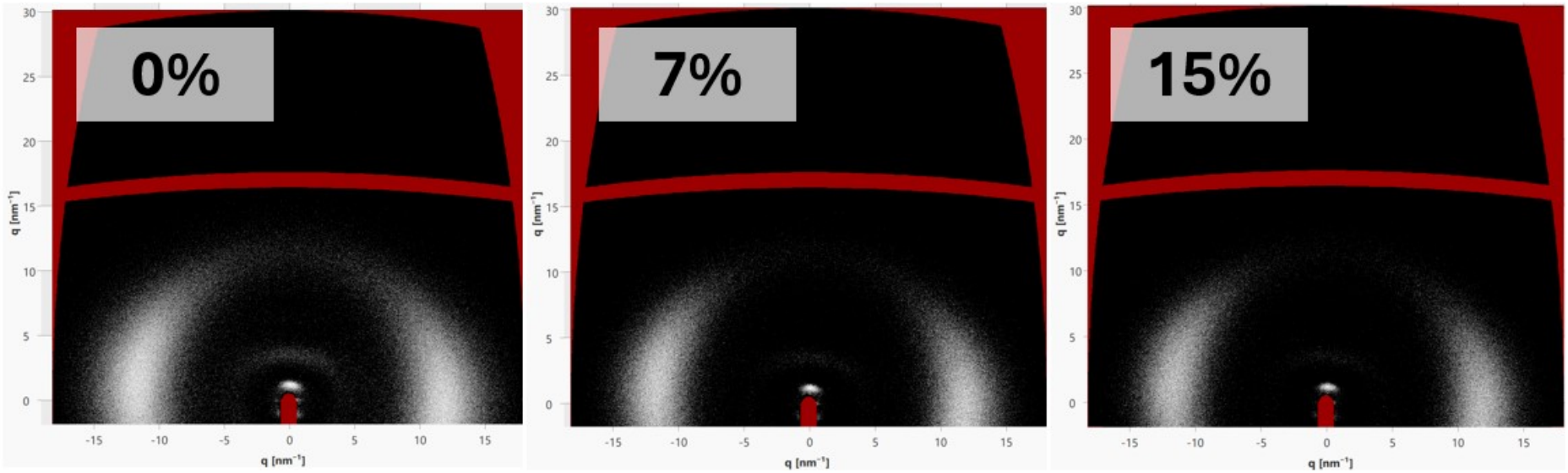

Figure S6 *- Representative 2D X-ray scattering patterns as a function of strain for the M1 LCE, showing 0%, 7% and 15% applied strain perpendicular to the director /layer normal*

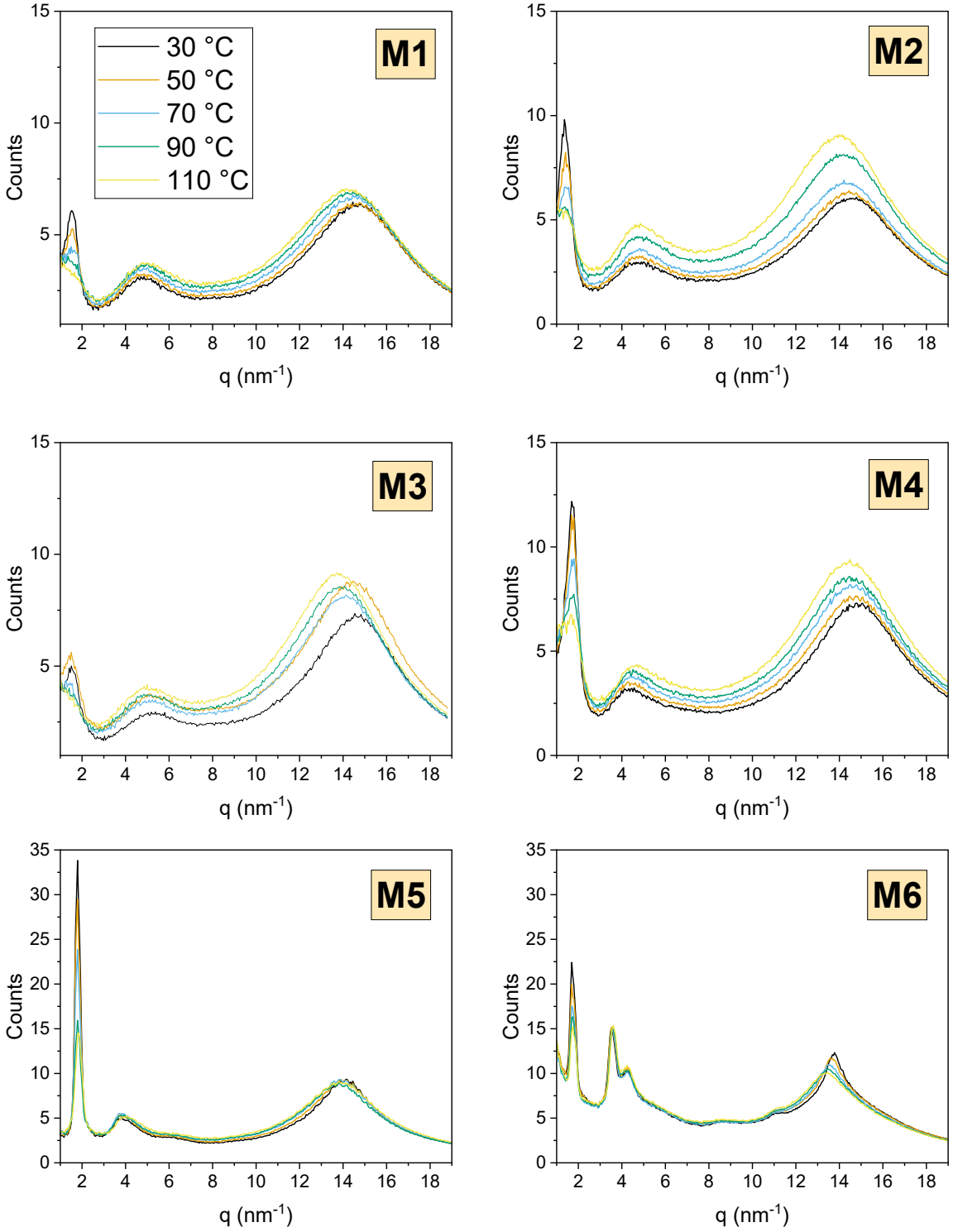

Figure S7 *– One dimensional radial integration for the X-ray scattering profile of each LCE. In all cases, there is a reduction in the intensity of the (001) Bragg reflection (around 2 nm^{-1}) as temperature increases, indicating a reduction in order.*

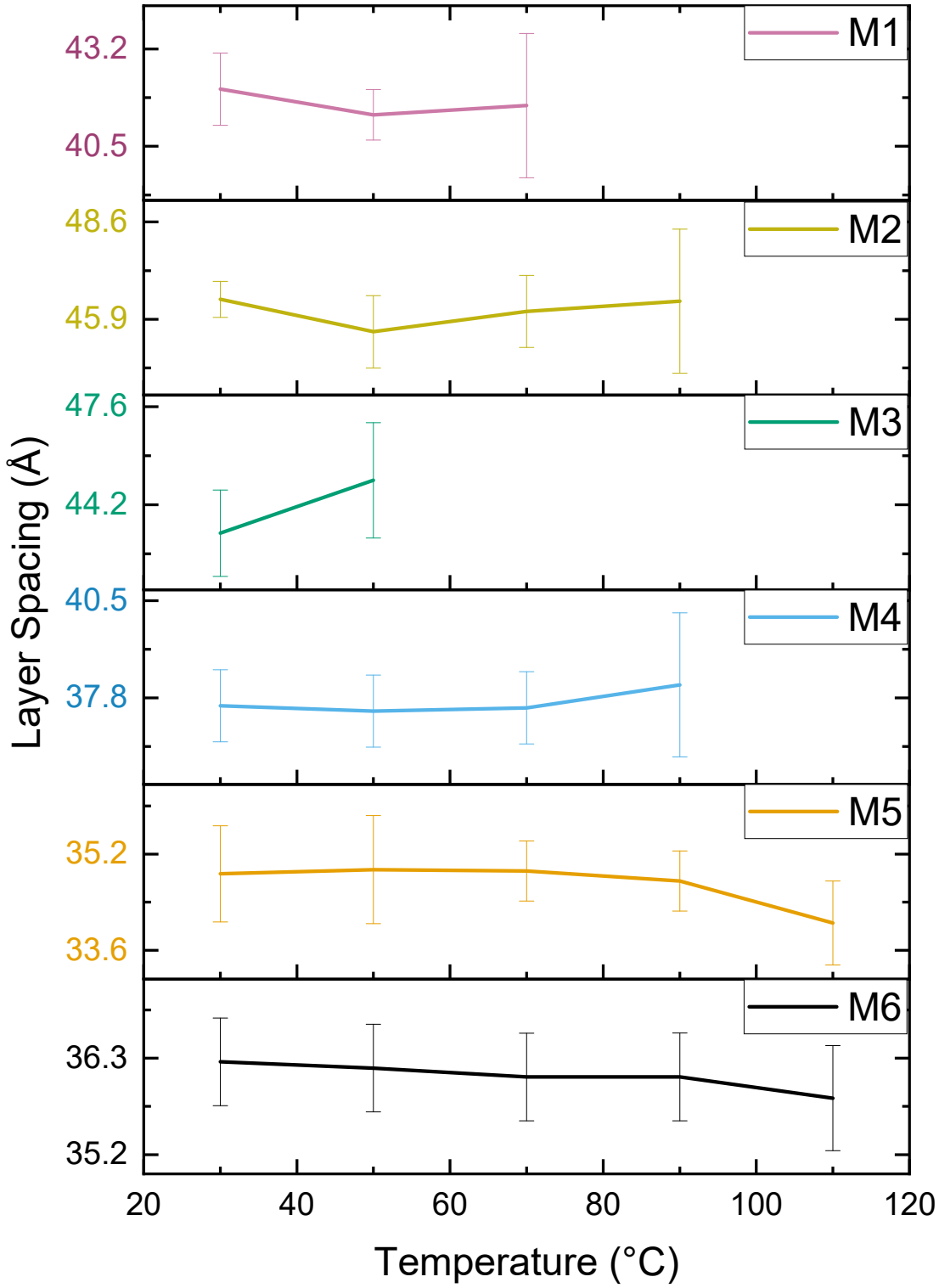

Figure S8 *- The effect of temperature on the smectic layer spacing in the LCE samples. Peak position is determined from a Gaussian fit to the data. At elevated temperatures for M1-M4, the signal to noise gave poor Gaussian fit, hence those data points are not included here. However, inspection of the 2D data,* ***Figure S6****, shows no discernible change in peak position.*

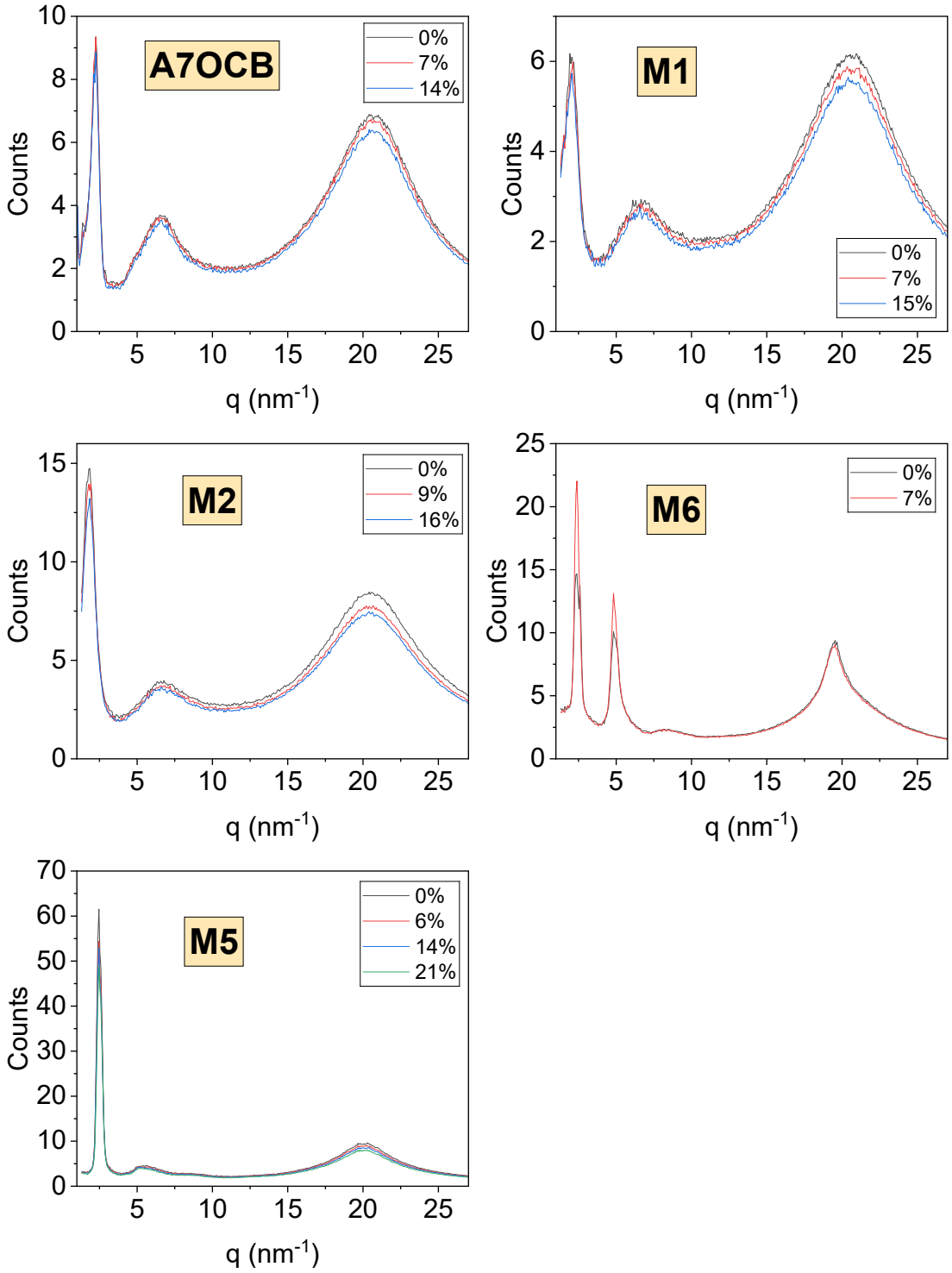

Figure S9 *- One dimensional radial integration for the X-ray scattering profile of representative LCE samples when subject to an applied strain perpendicular to the director/layer normal, with the legend detailing the extent of the strain applied. In all cases,*

no significant differences in the scattering patterns are observed, suggesting no layer spacing change or change in order are observed.

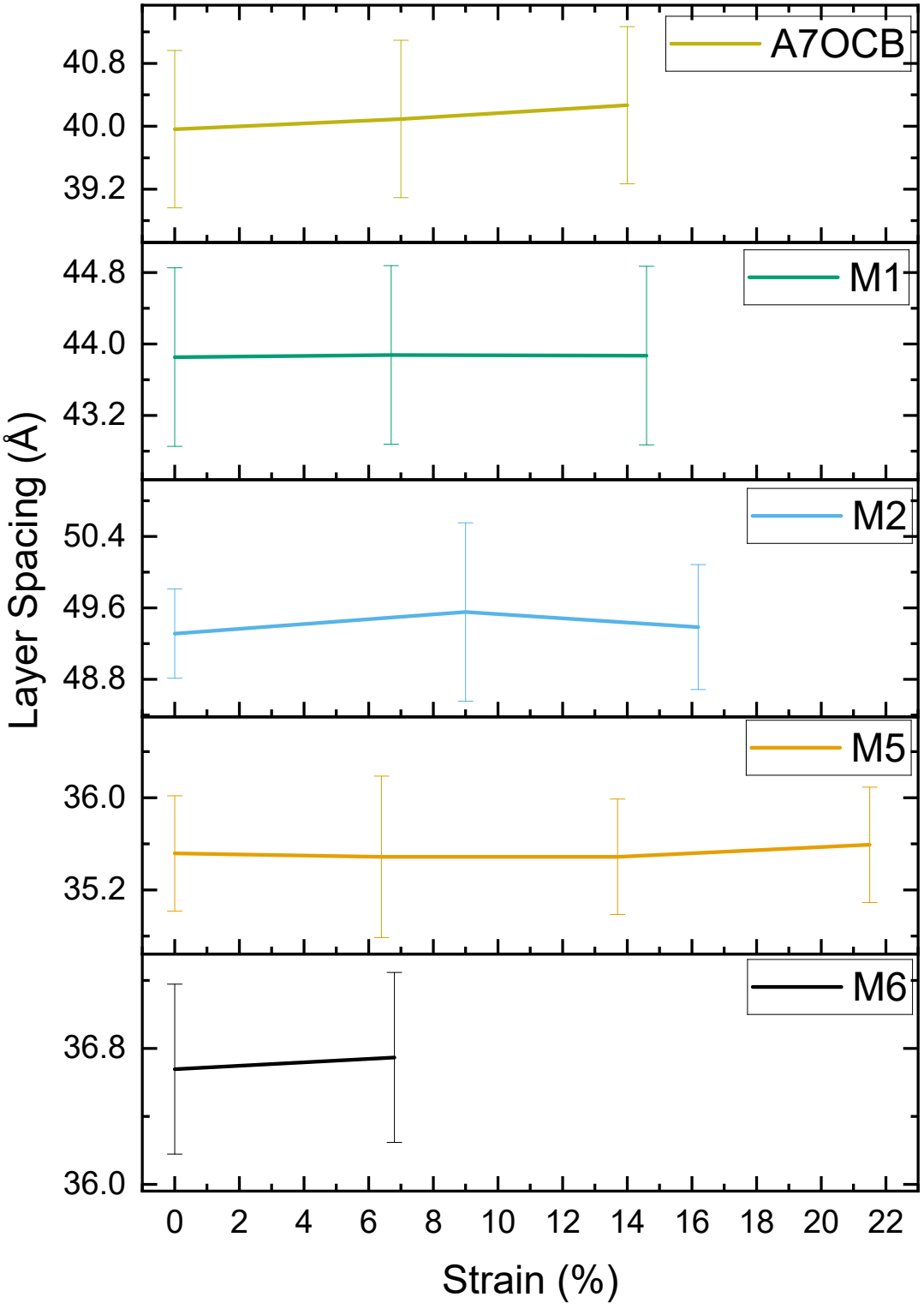

Figure S10 *– The effect of an applied strain perpendicular to the director/layer normal on the smectic layer spacing observed for the samples made with* ***A7OCB****,* ***M1****,* ***M2****,* ***M5*** *and* ***M6****.*

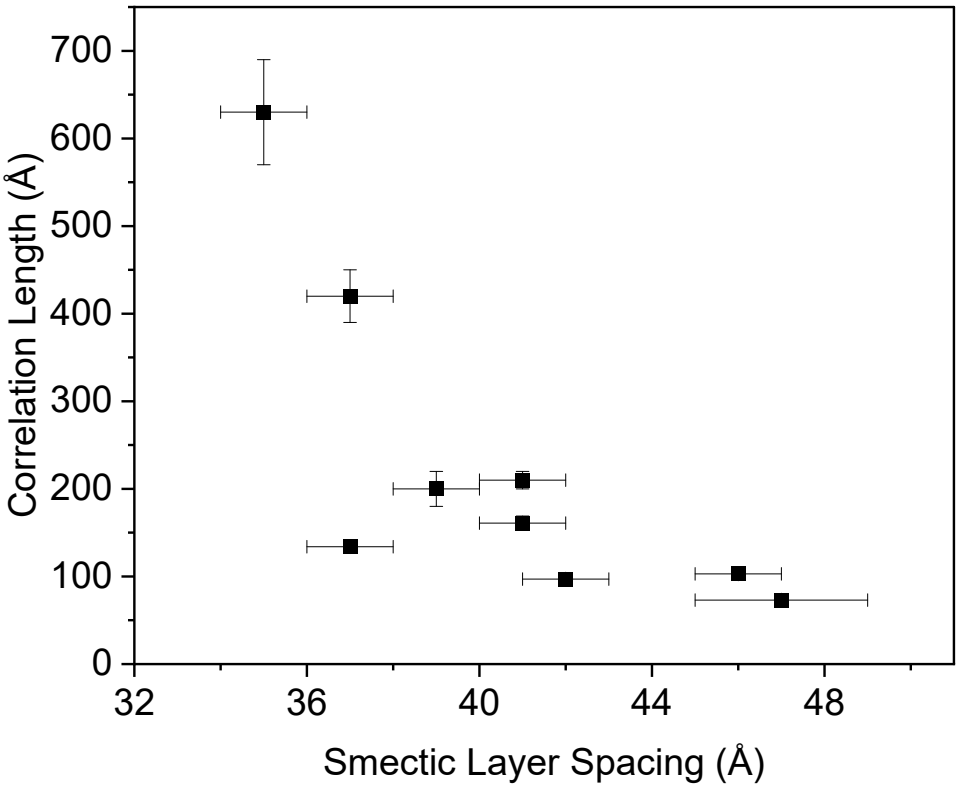

Figure S11 *- The correlation length plotted as a function of the smectic layer spacing for this series of LCEs. We clearly observe an increasing correlation length as the layer spacing decreases for this family of materials.*

Differential Scanning Calorimetry – Cured LCEs

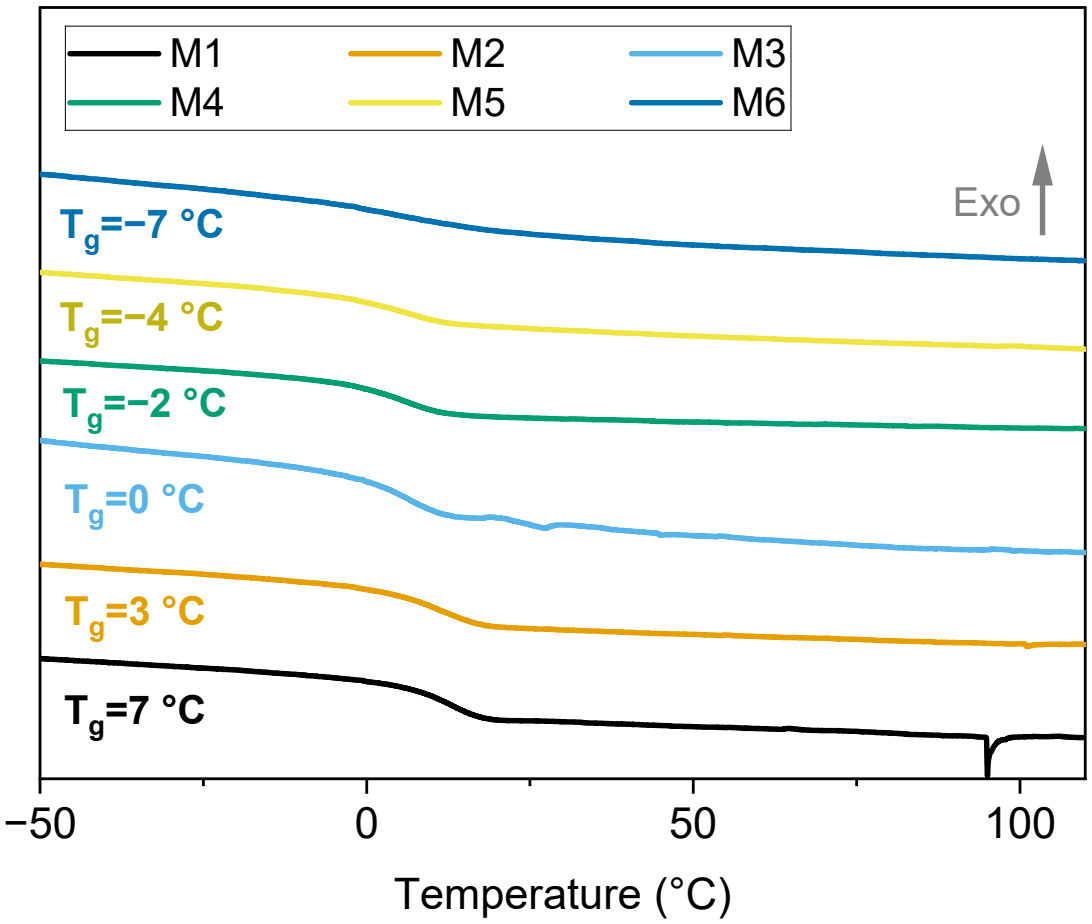

Figure S12 *– Example heating cycles from the DSC thermograms of each LCE sample, with samples heated at a rate of 10 °C/min. All T_g values shown are onset values.*

Table S1 *– Glass transition temperatures (T_g) for each LCE.*[†]

Monomer	T_g (°C)
M1	7
M2	3
M3	0
M4	-2
M5	-4
M6	-7

[†]All values are quoted as onset values on heating at 10 °C/min.

Differential Scanning Calorimetry – Uncured Precursor Mixtures

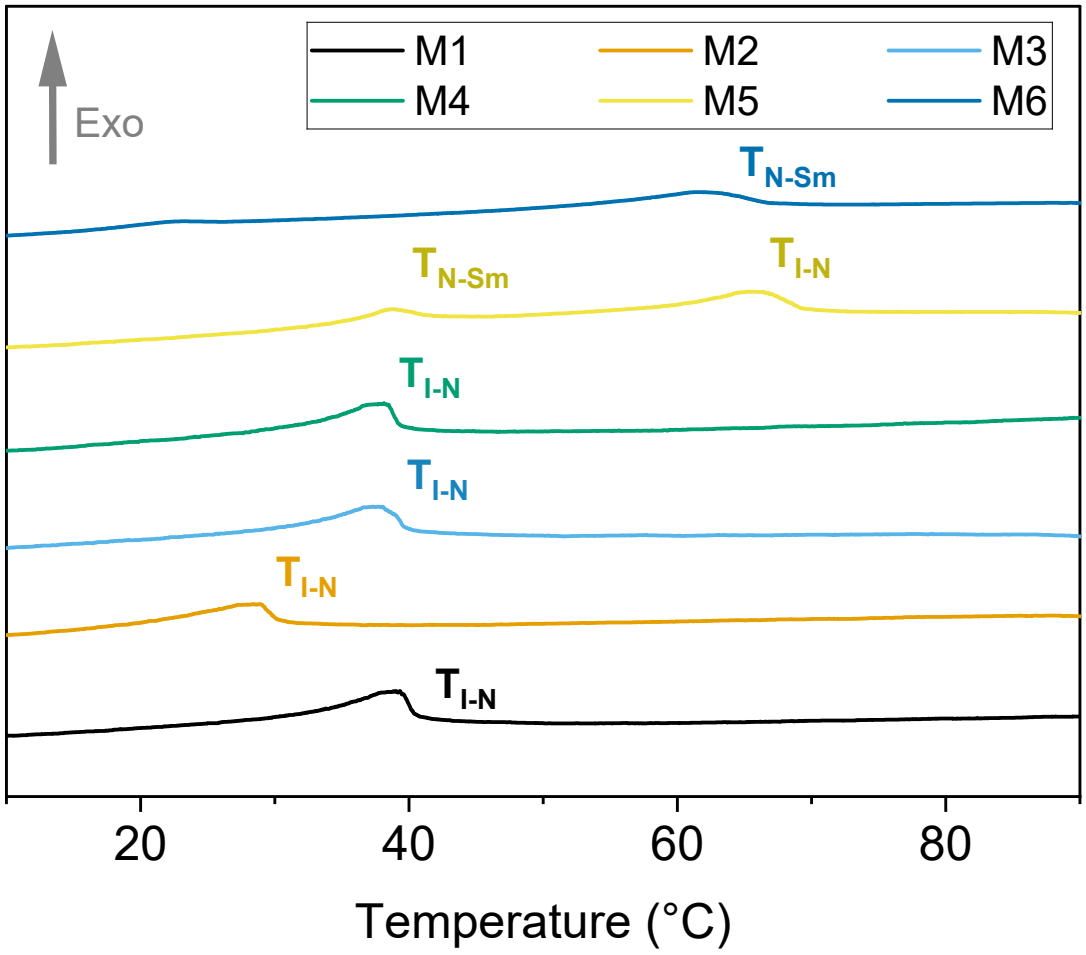

Figure S13 *– DSC thermograms to show the phase transitions of the LCE precursor mixtures. POM confirmed the phase assignations.*

Layer Compression Modulus Fits

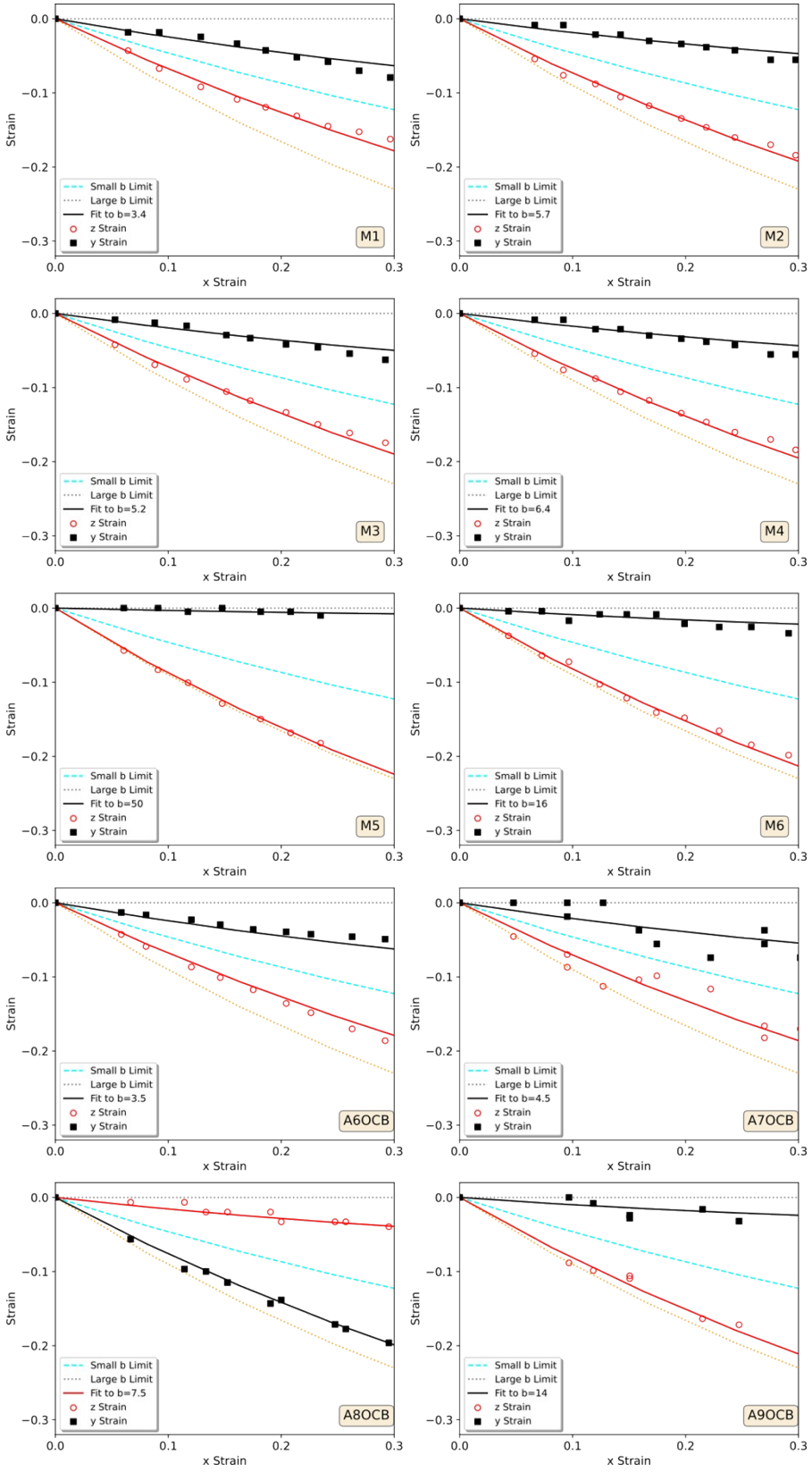

Figure S14 *– The strain response in the principal directions of the sample, the dotted and dashed lines represent the large band smallb limits respectively. A fit was performed using* ***Equation (1)*** *(in article text) to determine the value of b.*

Tensile Measurements

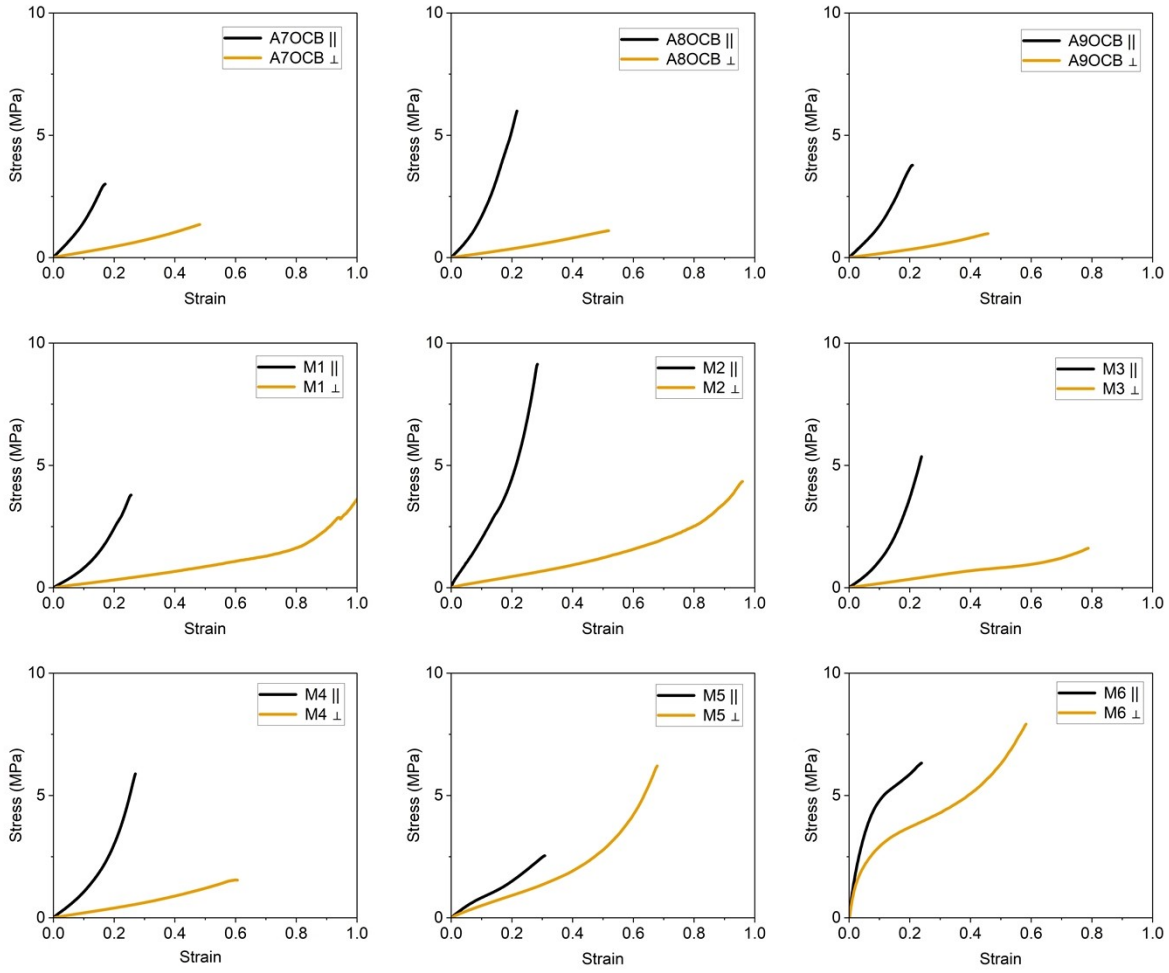

Figure S15 *Stress-strain plots for each LCE, comparing the behaviour when strain is applied parallel (||) and perpendicular (⊥) to the layer normal/director. In all cases, data were recorded at 22 °C.*

References

1 D. T. Kennedy, J. D. Hoang, M. F. Toney and T. J. White, *Macromolecules*, 2024, **57**, 10032–10040.

2 D. Mistry, S. D. Connell, S. L. Mickthwaite, P. B. Morgan, J. H. Clamp and H. F. Gleeson, *Nat Commun*, 2018, **9**, 5095.

3 T. Raistrick, Z. Zhang, D. Mistry, J. Mattsson and H. F. Gleeson, *Phys Rev Res*, 2021, **3**, 023191.